1-1-2014

Study on vanadium substitution to iron in Li2FeP 2O7 as cathode material for lithium-ion batteries

Jiantie Xu
University of Wollongong, jx307@uowmail.edu.au

Shulei Chou
University of Wollongong, shulei@uow.edu.au

Qinfen Gu
Australian Synchrotron Company

M F. Md Din
University of Wollongong, mfmd999@uowmail.edu.au

Hua-Kun Liu
University of Wollongong, hua@uow.edu.au

See next page for additional authors

Study on vanadium substitution to iron in Li2FeP 2O7 as cathode material for lithium-ion batteries

Abstract

A series of Li2Fe1-3x/2VxP 2O7 (x = 0, 0.025, 0.05, 0.075, and 0.1) cathode materials for LIBs were prepared by the sol-gel method. Structural characterization of Li2Fe1-3x/2VxP2O7 (x = 0, 0.025, 0.05, 0.075, and 0.1) samples was conducted by synchrotron X-ray diffraction. The morphology and oxidation states of Fe2+ and V 3+ in the Li2Fe1-3x/2VxP 2O7 samples were confirmed by scanning electron microscopy and magnetic susceptibility measurements, respectively. The electrochemical measurements indicated that Li2Fe1-3x/2VxP 2O7 (x = 0.025) delivered the higher reversible capacity of 79.9 mAh g-1 at 1 C in the voltage range of 2.0 - 4.5 V with higher 77.9% capacity retention after 300 cycles than those of Li 2FeP2O7 (48.9 mAh g-1 and 72.6%). Moreover, the rate capability of Li2Fe1-3x/2V xP2O7 (x = 0.025) were also significantly enhanced through vanadium substitution to iron of Li2Fe 1-3x/2VxP2O7. The vanadium substituted to Fe2 site of Li2FeP2O7 decreases Li occupying the Li5 position in the FeO5 unit, leading to a low degree exchange between Li and Fe in the MO5 (M = Li and Fe). The low degree cation disorder was beneficial to lithium-ion extraction/insertion during the charge-discharge process and hence enhances the capacity and rate capability.

Keywords

study, vanadium, substitution, iron, batteries, li2fep, ion, 2o7, cathode, material, lithium

Disciplines

Engineering | Physical Sciences and Mathematics

Publication Details

Xu, J., Chou, S., Gu, Q., Md Din, M. F., Liu, H. & Dou, S. (2014). Study on vanadium substitution to iron in Li2FeP 2O7 as cathode material for lithium-ion batteries. Electrochimica Acta, 141 195-202.

Authors

Jiantie Xu, Shulei Chou, Qinfen Gu, M F. Md Din, Hua-Kun Liu, and S X. Dou

Study on Vanadium Substitution to Iron in $Li_2FeP_2O_7$ as Cathode Material for Lithium-ion Batteries

Jiantie Xu [a], *Shu-Lei Chou* [a*], *Qin-Fen Gu* [b], Md-Din Muhamad [a,b], *Hua-Kun Liu*[a] *and Shi-Xue Dou* [a]

[a]*Institute for Superconducting and Electronic Materials, University of Wollongong, Wollongong, NSW 2522, Australia*

[b]*Australian Synchrotron, 800 Blackburn Rd, Clayton 3168, Australia*

* Corresponding author email address: shulei@uow.edu.au

Abstract

A series of $Li_2Fe_{1-3x/2}V_xP_2O_7$ (x = 0, 0.025, 0.05, 0.075, and 0.1) cathode materials for LIBs were prepared by the sol-gel method. Structural characterization of $Li_2Fe_{1-3x/2}V_xP_2O_7$ (x = 0, 0.025, 0.05, 0.075, and 0.1) samples was conducted by synchrotron X-ray diffraction. The morphology and oxidation states of Fe^{2+} and V^{3+} in the $Li_2Fe_{1-3x/2}V_xP_2O_7$ samples were confirmed by scanning electron microscopy and magnetic susceptibility measurements, respectively. The electrochemical measurements indicated that $Li_2Fe_{1-3x/2}V_xP_2O_7$ (x = 0.025) delivered the higher reversible capacity of 79.9 mAh g^{-1} at 1 C in the voltage range of 2.0 - 4.5 V with higher 77.9% capacity retention after 500 cycles than those of $Li_2FeP_2O_7$ (48.9 mAh g^{-1} and 72.6%). Moreover, the rate capability of $Li_2Fe_{1-3x/2}V_xP_2O_7$ (x = 0.025) were also significantly enhanced through vanadium substitution to iron of $Li_2Fe_{1-3x/2}V_xP_2O_7$. The vanadium substituted to Fe2 site of $Li_2FeP_2O_7$ decreases Li occupying the Li5 position in the FeO5 unit, leading to a low degree exchange between Li and Fe in the MO5 (M = Li and Fe). The low degree cation disorder was beneficial to lithium-ion extraction/insertion during the charge-discharge process and hence enhances the capacity and rate capability.

1. Introduction

$LiMPO_4$ (M = Fe, Co, Ni, Mn, and combinations thereof)) compounds have been considered to be among the most promising cathode materials for lithium-ion batteries intended for applications in electric vehicles (EVs) or renewable energy systems, due to their excellent electrochemical performance, low cost, and environmental friendliness. $LiMPO_4$ (M = Fe, Co, Ni, Mn, and combinations thereof)) compounds have stable three-dimensional (3D) frameworks containing PO_4 polyanions with strong covalent bonds, as well as M^{2+}/M^{3+} redox couples at high voltage (> 3.4 V), and thus offer high energy densities, long cycle life, excellent thermal stability, and high operating safety [1-4]. Recently, the pyrophosphates $Li_2MP_2O_7$ (M = Fe, Mn, and Co), which contain P_2O_7 polyanions formed by two PO_4 units sharing one O-O edge, have also been identified as cathode materials for lithium-ion batteries [5-18]. $Li_2FeP_2O_7$ prepared by conventional solid-state synthesis at 600 °C delivered a reversible specific capacity of around 110 mAh g^{-1} with an operating voltage of about 3.5 V at 0.05 C in the voltage range of 2.0 - 4.5 V [6]. Compared to its couterpart $LiFePO_4$ (~ 166 mAh g^{-1}), $Li_2FeP_2O_7$ has a lower theoretical capacity (~ 110 mAh g^{-1}) because of the relatively heavy weight of the pyrophosphate and the extraction of only one electron per formula unit. However, $Li_2FeP_2O_7$ showed a slightly higher operating voltage (~ 3.5 V vs. ~ 3.4 V) and lower synthesis temperature than $LiFePO_4$. Not only for these advantages, but also due to the possibilities of extracting two electrons from $Li_2MP_2O_7$ (*e.g.*, M = Mn) with a theoretical capacity of ~ 220 mAh g^{-1}, the pyrophosphates $Li_2MP_2O_7$ (M = Fe, Co, Ni, Mn, and combinations thereof)) have already received more attention as promising high voltage cathode materials for lithium-ion batteries [5-18].

So far, $Li_2FeP_2O_7$ as cathode for LIBs suffers from the low rate capability or poor cycling stability because of its low electronic and ionic conductivity [5-18]. As the counterpart of $Li_2FeP_2O_7$, $LiFePO_4$ also showed the low electronic and ionic conductivity [3, 6, 7]. However,

over the past decades, simple and effective techniques, including carbon coating, morphology control, particle size reduction, and aliovalent doping, have been made to overcome this obstacle to the application of $LiFePO_4$ [1-4]. Among these techniques, aliovalent doping was intensively investigated as one of most effective techniques to improve the electrochemical performance of $LiFePO_4$, as the electronic and ionic conductivity of $LiFePO_4$ was critically increased by several orders of magnitude through a small amount of aliovalent doping [19, 20]. Among the many aliovalent elements, active vanadium element was widely employed as a dopant in $LiFePO_4$ because of its various oxidation states (2^+, 3^+, 4^+, 5^+) [21-36]. Despite the enhanced electrochemical performance through vanadium doping, there is still no agreement on the explanation. The reasons given for the improvement in the electrochemical performance vary from replacement of Fe, Li, or P by vanadium so as to enlarge lithium or electron pathways [24, 25, 28-30], to no vanadium substitution entering into the $LiFePO_4$ host structure [26], or formation of an impurity phase V_2O_3 coating [27].

To date, there is no report on aliovalent doping in $Li_2MP_2O_7$ (M = Fe, Co, Ni, Mn, and combinations thereof)) compounds. Therefore, a study of aliovalent doping in $Li_2MP_2O_7$ could provide new insights to understand the mechanism behind the effects of aliovalent doping on the electrochemical performance of pyrophosphates. Here, we prepared a series of V-incorporated $Li_2FeP_2O_7$ samples by the sol-gel method, assisted by citric acid and sucrose as the carbon sources and reductive agent. The detailed structures, magnetic properties, and electrochemical performance of V-incorporated $Li_2FeP_2O_7$ were investigated. We found that $Li_2Fe_{1-3x/2}V_xP_2O_7$ (x = 0.025) delivered the higher reversible capacity of 79.2 mAh g^{-1} at 1 C in the voltage range of 2.0 - 4.5 V with higher 75.8% capacity retention after 500 cycles than those $Li_2Fe_{1-3x/2}V_xP_2O_7$ (x = 0) (49 mAh g^{-1} and 65.8%, respectively). The improved electrochemical performance for $Li_2Fe_{1-3x/2}V_xP_2O_7$ (x = 0.025) can be attributed to vanadium substitution into its Fe sites by SXRD. The vanadium substituted on Fe2 sites of $Li_2FeP_2O_7$ is

beneficial to decrease Li occupying the Li5 position in the FeO5 unit, leading to a low degree exchange between Li and Fe in the MO5 (M = Li and Fe). The low degree cation disorder could facilitate lithium ion extraction/insertion, and hence enhance the capacity and rate capability.

2. Experimental section

2.1. Material synthesis

The $Li_2Fe_{1-3x/2}V_xP_2O_7$ (x = 0, 0.025, 0.05, 0.075, and 0.1) compounds were prepared by the citric acid (CA) assisted sol-gel method from the starting materials LiH_2PO_4, $(CH_3COO)_2Fe$, NH_4VO_3, and sucrose. The molar ratio of Li/Fe/V/P/sucrose was 2 : (1 - 3x/2) : x : 2 : 0.34 (x = 0, 0.025, 0.05, 0.075, and 0.1). The starting materials were dissolved in distilled water, and then citric acid was added to this solution under stirring (molar ratio of CA/sucrose = 1.5 : 1). Each solution was heated gently with continuous stirring to remove the excess water at 80 °C in a thermostatic water bath to obtain a viscous gel, which was then dried in a vacuum oven at 80 °C to yield a xerogel. The xerogels were then ground, heated to 600 °C at a heating rate of 5 ^{o}C min^{-1} in a tube furnace, and then kept at that temperature for 10 h under flowing high purity argon atmosphere, followed by natural cooling to room temperature.

2.2. Materials characterization

The phase identification of the $Li_2Fe_{1-3x/2}V_xP_2O_7$ (x = 0, 0.025, 0.05, 0.075, and 0.1) compounds was carried out by synchrotron X-ray diffraction (SXRD, Melbourne, Australian Synchrotron). The SXRD data were collected over a 2θ range of 3 - 80° with a step size of 0.0038°, using a wavelength of 0.825 Å. The morphology and particle size of the $Li_2Fe_{1-3x/2}V_xP_2O_7$ sample were characterized by scanning electron microscopy (SEM) and transmission electron microscopy (TEM), using JSM-7500FA and JEOL JEM-2011

instruments, respectively. The specific surface area was measured by the 15 point N_2 absorption Brunauer-Emmett-Teller (BET) method using a Quanta Chrome Nova 1000. The carbon content of the $Li_2Fe_{1-3x/2}V_xP_2O_7$ (x = 0, 0.025, 0.05, 0.075, and 0.1) was characterized by thermogravimetric analysis (TGA, Mettler Toledo) in air over the temperature range of 50 - 800 °C with a ramp rate of 10 °C min^{-1}. The carbon content was also verified by Vario EL (Elementar, Germany) CHNS Elemental Analyzer. The magnetic measurements were carried out using a 14 T physical properties measurement system (PPMS), equipped with a vibrating sample magnetometer (VSM), over a wide temperature range from 2 to 340 K in a 100 Oe magnetic field. The electronic conductivity measurement of $Li_2Fe_{1-3x/2}V_xP_2O_7$ (x = 0, 0.025, 0.05, 0.075, and 0.1) powders was adopted with a Jandel RM3 four-point probe measurement system at room temperature. The specimens used for electronic conductivity measurement were disk-shaped pellets with 8 mm in diameter and 1.5 mm in thickness.

2.3. Electrochemical measurements

The electrochemical characterization of the $Li_2Fe_{1-3x/2}V_xP_2O_7$ (x = 0, 0.025, 0.05, 0.075, and 0.1) samples was carried out using coin cells. CR 2032 coin-type cells were assembled in an Ar filled glove box by stacking the electrodes on an Al foil as the working electrode, with an Li foil as the counter electrode and reference electrode, a porous polypropylene film as separator, and 1 M $LiPF_6$ in a 1 : 2 (v/v) mixture of ethylene carbonate (EC) and diethyl carbonate (DEC) as the electrolyte. The cells were galvanostatically charged and discharged using an automatic battery tester system (Land®, China) in the voltage range of 2.0 - 4.5 V at various current densities. Electrochemical impedance spectroscopy (EIS) measurements were performed using a Biologic VMP3 electrochemical workstation in the frequency range from 1 M Hz to 10 mHz.

3. Results and discussions

The synchrotron X-ray powder diffraction (SXRD) and refinement data for $Li_2Fe_{1-3x/2}V_xP_2O_7$ (x = 0, 0.025, 0.05, 0.075, and 0.1) are shown in Figure 1. There is no visible impurity phase in the SXRD patterns of $Li_2Fe_{1-3x/2}V_xP_2O_7$ ($x \leq 0.05$), indicating that V is doped into the host lattice. For the samples with $x \geq 0.075$, the diffraction peaks for $LiVP_2O_7$ secondary phase is observed. The reasonably small weighted profile R-factor, R_{wp}, (1.98%, 2.08%, and 2.43%), for Rietveld refinement, further confirmed that single-phase $Li_2Fe_{1-3x/2}V_xP_2O_7$ (x = 0, 0.025, and 0.05) with a monoclinic crystal structure ($P2_1/c$ symmetry) is obtained through our experimental process, respectively. The quantitative analysis from the Rietveld refinement results revealed that ~ 4.5 wt. % and ~ 9.7 wt. % $LiVP_2O_7$ was present in the $Li_2Fe_{1-3x/2}V_xP_2O_7$ (x = 0.075) and $Li_2Fe_{1-3x/2}V_xP_2O_7$ (x = 0.1) samples, respectively. The respective cell parameters of $Li_2Fe_{1-3x/2}V_xP_2O_7$ (x = 0, 0.025, 0.05, 0.075, and 0.1) are given in Table 1. As shown in Table 1 and Figure 2, the *a*, *b*, *c* lattice parameters and the unit cell volume all decreased linearly with increasing vanadium concentration because of the smaller ionic radii of V (0.74 Å) species substituting for Fe species with larger ionic radii (0.76 Å) in the $Li_2FeP_2O_7$.

A schematic illustration of the SXRD refined structures of $Li_2Fe_{1-3x/2}V_xP_2O_7$ is shown in Figure 3. In $Li_2MP_2O_7$ (M = Mn or Fe) crystal structure [6, 14], all of the Li, M, P, and O atoms occupy positions with different coordinates, i.e., there are five Li positions (Li1-Li5), three M sites (M1-M3), four P positions (P1-P4), and fourteen O sites (O1-O14). As shown in Figure 3(a), the apparent tunnels suitable for passing lithium (accommodating Li2 and Li4 site atoms) in $Li_2Fe_{1-3x/2}V_xP_2O_7$ are stacked along the *c*-axis through the $[FeP_2O_7]$ network in the *ab*-plane, which is composed of Fe_2O_9 and P_2O_7 units. Figure 3(b) indicates that the metal atoms (Li, Fe, V) in $Li_2Fe_{1-3x/2}V_xP_2O_7$ are located in the three edge-sharing units: fully occupied MO_6 octahedra (M = Fe1 site) and LiO_5 trigonal-bipyramids, along with FeO_5

trigonal-bipyramids that are statically occupied by residual Fe. It should be noted that the FeO_5 bipyramidal sites (Fe2 site) are partially occupied by lithium (Li5 site), while the LiO_5 bipyramidal sites (Li1 site) are also partially occupied by iron (Fe3 site). According to the smaller reliability factor of the SXRD refinement results, we found that the substitution by V preferentially took place on the FeO_5 rather than on FeO_6 (Fe1 site). Furthermore, since the sum of the sites where vanadium could occupy MO_5 (M = Li and Fe) was fixed to the stoichiometric amount, the reliability factors of the refinement were decreased with an increasing vanadium proportion in the FeO_5, indicating that the vanadium atoms preferentially occupy the Fe2 site in the FeO_5 rather than the Li1 site in the LiO_5. Therefore, the vanadium substituted on Fe2 site of $Li_2FeP_2O_7$ is beneficial to decrease Li occupying the Li5 position in the FeO5 unit, leading to a low degree exchange between Li and Fe in the MO5 (M = Li and Fe). Samples with a low degree of cation disorder (lithium atom and metal atom are exchanged in each site) in layered metal oxides as cathode materials, such as $LiNiO_2$, $LiNi_{1/3}Mn_{1/3}Co_{1/3}O_2$, and $LiNi_{0.2}Mn_{0.4}Co_{0.4}O_2$, have shown improved electrochemical performance [37-40]. Therefore, it is expected that the electrochemical performance of $Li_2Fe_{1-3x/2}V_xP_2O_7$ could be enhanced by vanadium substitution on the Fe2 sites.

The magnetic properties are widely used to determine magnetic interactions, sample purity, transition metal oxidation states, and structural ordering [29, 35, 36, 41]. The magnetic susceptibility, χ, of $Li_2Fe_{1-3x/2}V_xP_2O_7$ (x = 0, 0.025, 0.05) from 2 to 300 K is shown in Figure 4(a). Typical ferrimagnetic behaviour can be found in the low temperature range (Figure 4(a)), which is similar to the previous report on the vanadium doping $LiFePO_4$ [29]. The Curie Weiss law, $\chi - \chi^0 = C_M/(T-\Theta)$, where χ^0 is the temperature-independent contribution to the susceptibility, T is the absolute temperature, C_M is the material dependent Curie constant, and Θ is the Weiss constant, was used to fit the paramagnetic part of the dependence (inset of Figure 4(a)). The magnetic parameters of $Li_2Fe_{1-3x/2}V_xP_2O_7$ (x = 0, 0.025,

and 0.05) calculated from the fitted inverse susceptibility curves (inset of Figure 4(a)) and the dM/dT curves (inset of Figure 4(b)) are listed in Table 2. As shown in Table 2, with increasing vanadium content, the absolute value of the Néel temperature, T_N, slightly decreases, which is consistent with weakening of the antiferromagnetic exchange after vanadium substitution, because the V^{2+} ($3d^3$) and V^{3+} ($3d^2$) states have a lower number of unpaired electrons than Fe^{2+} ($3d^6$) [29]. Consequently, the Curie constant also decreases with vanadium substitution, giving a lower effective total magnetic moment. Furthermore, for $Li_2FeP_2O_7$, the experimental magnetic moment, $\mu_{experiment}$ = 4.88 μB, in excellent agreement with the value of 4.90 μB that is expected for the $3d^6$ Fe^{2+} ion. The small difference between the theoretical and experimental moments confirms the presence of Fe^{2+} and V^{3+} throughout the entire series.

Since the preparation method is the same, and the difference in the vanadium content is small, the morphology is similar for all the samples. Here, we select the scanning electron microscope (SEM) and transmission electron microscope (TEM) images of $Li_2Fe_{1-3x/2}V_xP_2O_7$ (x = 0.025). As shown in Figure 5(a) and (b), the $Li_2Fe_{1-3x/2}V_xP_2O_7$ (x = 0.025) sample consists of small particles with a wide size distribution in the range of 100 nm - 1 μm. Furthermore, as shown in Figure 5(c) and (d), the TEM images of $Li_2Fe_{1-3x/2}V_xP_2O_7$ (x = 0.025) show a ~ 3.5 nm amorphous carbon coating on the surfaces of highly crystallized $Li_2Fe_{1-3x/2}V_xP_2O_7$ (x = 0.025), which was further supported by the corresponding Fourier transform image (inset of Figure 5(d)). To identify the carbon content of $Li_2Fe_{1-3x/2}V_xP_2O_7$ $_{3x/2}V_xP_2O_7$ (x = 0, 0.025, 0.05, 0.075, and 0.1), the thermogravimetric analysis (TGA) was employed. As shown in Figure 6(a), the TGA curves of $Li_2Fe_{1-3x/2}V_xP_2O_7$ $_{3x/2}V_xP_2O_7$ (x = 0, 0.025, 0.05, 0.075, and 0.1) are divided into four parts in the temperature range of 80 to 800 °C: total mass change (Δm_{total}) over the whole process, total gasification of carbon (Δm_c), and oxidation of $Li_2Fe_{1-3x/2}V_xP_2O_7$ (Δm_{L1}, Δm_{L2}) ($Fe^{2+} \rightarrow Fe^{3+}$ in the temperature range of 200

- 400 °C and $V^{3+} \rightarrow V^{5+}$ in the temperature range of 450 - 600 °C). Therefore, the carbon content of $Li_2Fe_{1-3x/2}V_xP_2O_7$ (x = 0) can be estimated from the following Equations (1 and 2):

$$\Delta m_{total} = -\Delta m_c + \Delta m_{L1} + \Delta m_{L2} \quad (1)$$

$$\Delta m_{L2} = k \times \text{wt. \% } (LiVP_2O_7) \quad (2)$$

Where, we assume that the constant k = 0.0784 for the $LiVP_2O_7$ [42]; wt. % ($LiVP_2O_7$) is the weight percentage in the $Li_2Fe_{1-3x/2}V_xP_2O_7$ (x = 0.075, 0.1) samples (~ 4.5 wt. % for $Li_2Fe_{0.8675}V_{0.075}P_2O_7$ and ~ 9.7 wt. % for $Li_2Fe_{0.85}V_{0.1}P_2O_7$). Therefore, according to Equations (1 and 2), for x = 0.0, Δm_c = - 4.95 wt. %, where Δm_{total} = 5.3 wt. %, Δm_{L1} = 0.55 wt. %, and Δm_{L2} = 0.0 wt. %. In the same way, the carbon content of $Li_2Fe_{1-3x/2}V_xP_2O_7$ (x = 0.025, 0.05, 0.075, and 0.1) is calculated to be 5.02 wt. %, 4.91 wt. %, 4.81 wt. %, and 4.75 wt. %, respectively. The carbon content agrees well with the results from CHNSO measurement (5.32 wt. % for x = 0, 5.18 wt. % for x = 0.025, 4.92 wt. % for x = 0.05, 5.33 wt. % for x = 0.075 and 4.87 wt. % for x = 0.1). Meanwhile, as shown in Figure 6(b), a highly exothermal reaction of our samples was observed at 475 ^oC in the differential scanning calorimetry (DSC) curves, which is smaller than that in a previous report at 510 ^oC [14]. The specific surface areas of all the samples were measured by the Brunauer-Emmett-Teller method and are in a range of 2.2 to 3.6 $m^2 g^{-1}$.

Initial charge-discharge curves and the cycling performance of $Li_2Fe_{1-3x/2}V_xP_2O_7$ (x = 0, 0.025, 0.05, 0.075, and 0.1), measured in the voltage range of 2.0 - 4.5 V, are shown in Figure 7. As shown in Figure 7(a), the charge-discharge profile of the $Li_2FeP_2O_7$ agrees well with those reported previously [6, 7, 11]. $Li_2FeP_2O_7$ delivers a reversible capacity of 95.3 mAh g^{-1} at 0.1 C with a plateau at ~ 3.45 V, 86% of the theoretical capacity of 110 mAh g^{-1} ($Fe^{2+} \rightarrow Fe^{3+}$). There is a slight concurrent increase in the initial specific capacity of $Li_2Fe_{1-3x/2}V_xP_2O_7$ with increasing V-doping content (98.5 mAh g^{-1} for x = 0.025, 96.9 mAh g^{-1} for x = 0.05). As

V doping continues to increase, however, it results in the appearance of $LiVP_2O_7$ impurity in the $Li_2Fe_{1-3x/2}V_xP_2O_7$ (x = 0.075, 0.1), and the electrode polarization of $Li_2Fe_{1-3x/2}V_xP_2O_7$ (x = 0.075, 0.1) gradually increases, causing the initial capacity to drop to 75.8 mAh g^{-1} for x = 0.075, and 59.8 mAh g^{-1} for x = 0.1, respectively. The initial sharply fading capacity for $Li_2Fe_{1-3x/2}V_xP_2O_7$ (x = 0.075, 0.1) may arise from the change in cationic distribution due to possible structural deformation for the host structure and the effects of $LiVP_2O_7$ impurity. Compared to $Li_2FeP_2O_7$, the $LiVP_2O_7$ impurity showed poorer discharge-charge capability because of low electronic conductivity (~ 50 mAh g^{-1} in the voltage range of 2.0 – 4.5 V at 0.05 C), as well as significantly distorted structures after charge process [43]. To investigate the effects of V doping on the rate and cycling performance, $Li_2Fe_{1-3x/2}V_xP_2O_7$ (x = 0, 0.025, 0.05, 0.075, and 0.1) cells were charged and discharged for 105 cycles between 2.0 and 4.5 V at various current densities from 0.1 to 2 C in steps. As shown in Figure 7(b), at 0.1 C, the samples with V substitution on Fe sites (x = 0.025, 0.05) present similar discharge capacities to the pure sample (x = 0) during the cycling, however, there is a large decrease in the discharge capacities of the heavily V-doped samples ($x \geq 0.075$). With increasing C-rate (≥ 0.2 C), the $Li_2Fe_{1-3x/2}V_xP_2O_7$ (x = 0.025) showed the best rate capability among all the $Li_2Fe_{1-3x/2}V_xP_2O_7$ samples.

Figure 8 shows the relatively long-term cycling performances for the $Li_2Fe_{1-3x/2}V_xP_2O_7$ (x = 0, 0.025, 0.05, 0.075, and 0.1) electrodes measured at 1 C in the voltage range of 2.0 - 4.5 V. As can be seen, the $Li_2Fe_{1-3x/2}V_xP_2O_7$ samples exhibited different initial discharge capacities of 79.2 (x = 0.025), 66.0 (x = 0.05), 49.0 (x = 0), 37.8 (x = 0.075), and 26.9 (x = 0.1) mAh g^{-1}, respectively. After 500 cycles, the $Li_2Fe_{1-3x/2}V_xP_2O_7$ (x = 0, 0.025, 0.05, 0.075, and 0.1) cells could maintain the discharge capacities of 60 (x = 0.025), 42.1 (x = 0.05), 32.2 (x = 0), 24.8 (x = 0.075), and 15.2 (x = 0.1) mAh g^{-1} with initial capacity retention of 75.8%, 63.8%, 65.8%, 65.6% and 56.5%, respectively. The higher discharge capacity and capacity retention

observed for the $Li_2Fe_{1-3x/2}V_xP_2O_7$ (x = 0.025) indicate, once again, that the $Li_2Fe_{1-3x/2}V_xP_2O_7$ (x = 0.025) has the best cycling performance among $Li_2Fe_{1-3x/2}V_xP_2O_7$ (x = 0, 0.025, 0.05, 0.075, and 0.1). The enhanced electrochemical performance of this V-substituted sample (x = 0.025) is most likely related to its improved ionic conductivity.

Electrochemical impedance spectroscopy (EIS) was extensively used to investigate the ionic conductivity of the $Li_2Fe_{1-3x/2}V_xP_2O_7$ samples (Figure 9) [44]. The Nyquist plots were obtained from the $Li_2Fe_{1-3x/2}V_xP_2O_7$ (x = 0, 0.025, 0.05, 0.075, and 0.1) electrodes measured at 0.1 C in the voltage range of 2.0 - 4.5 V after 10 cycles in the discharge state of 3.4 V. The numerical value of the diameter of the semicircle on the Z_{re} axis is approximately equal to the charge transfer resistance (R_{ct}), which is an indicator of the charge-transfer kinetics. The fitting results are listed in Table 3. The R_{ct} values of $Li_2Fe_{1-3x/2}V_xP_2O_7$ (x = 0, 0.025, 0.05, 0.075, and 0.1) calculated from this model are 480.8, 262.9, 356.8, 2833, and 4392 Ω, respectively. The $Li_2Fe_{1-3x/2}V_xP_2O_7$ (x = 0.025) sample shows the lowest R_{ct} value, indicating the highest conductivity. The four-point probe measurement system was adopted to get the electronic conductivity of $Li_2Fe_{1-3x/2}V_xP_2O_7$ powders at room temperature. The conductivity are 2.92×10^{-5} S cm^{-1} (x = 0), 4.99×10^{-5} S cm^{-1}(x = 0.025), 3.57×10^{-5} S cm^{-1}(x = 0.05), 4.45×10^{-6} S cm^{-1}(x = 0.075), 2.92×10^{-6} S cm^{-1} (x = 0.1), further indicating the highest conductivity for $Li_2Fe_{1-3x/2}V_xP_2O_7$ (x = 0.025). The expanded volume or cell parameters are favourable for the passage of lithium-ions through the host structures [24, 25, 28-30]. However, the cell lattice parameters and unit cell volume of the $Li_2Fe_{1-3x/2}V_xP_2O_7$ samples decrease linearly with the V doping level, as shown in Table 1 and Figure 2. Therefore, it is suggested that the improved electronic conductivity are attributed to appropriate vanadium substitution in $Li_2Fe_{1-3x/2}V_xP_2O_7$ (x = 0.025, 0.05) to effectively decrease the exchange of lithium and Fe in the MO_5 (M = Li and Fe) trigonal-bipyramidal sites and facilitate lithium-ion extraction/insertion. When the vanadium doping is further increased ($x \geq 0.075$), the

increased vanadium doping results in possible distortion of the host structure and the presence of $LiVP_2O_7$, and thus dramatically decreases the specific capacity. As shown in Table 3, the EIS results are consistent with the results on the electrochemical performance of $Li_2Fe_{1-3x/2}V_xP_2O_7$ (x = 0, 0.025, 0.05, 0.075, and 0.1).

4. Conclusions

A series of $Li_2Fe_{1-3x/2}V_xP_2O_7$ (x = 0, 0.025, 0.05, 0.075, and 0.1) samples have been successfully prepared using the sol-gel method. Through synchrotron X-ray diffraction analysis, single phase $Li_2Fe_{1-3x/2}V_xP_2O_7$ with $x \leq 0.05$ is obtained, while the $Li_2Fe_{1-3x/2}V_xP_2O_7$ samples with $0.075 \leq x \leq 0.1$ show the secondary impurity phase $LiVP_2O_7$. The morphology and oxidation states of Fe^{2+} and V^{3+} in the $Li_2Fe_{1-3x/2}V_xP_2O_7$ were confirmed by scanning electron microscopy and magnetic susceptibility measurements, respectively. The electrochemical results indicated that the electrochemical performance could be significantly enhanced by vanadium substitution on the Fe sites of $Li_2Fe_{1-3x/2}V_xP_2O_7$ (x = 0.025, 0.05). The $Li_2Fe_{1-3x/2}V_xP_2O_7$ (x = 0.025) sample was found to deliver a higher reversible capacity of 79.9 mAh g^{-1} at 1 C in the voltage range of 2.0 - 4.5 V with higher 77.9% capacity retention after 500 cycles than that of those of $Li_2FeP_2O_7$ (49 mAh g^{-1} and 65.8%). The improved electrochemical performance for $Li_2Fe_{1-3x/2}V_xP_2O_7$ (x = 0.025) was attributed to that the vanadium substituted on Fe2 site of $Li_2FeP_2O_7$ decreases Li occupying the Li5 position in the FeO5 unit, leading to a low degree exchange between Li and Fe in the MO5 (M = Li and Fe). The low degree cation disorder was beneficial to lithium-ion extraction/insertion during the charge-discharge process, and hence enhances the capacity and rate capability.

5. Acknowledgements

Financial supports provided by the Australian Research Council (ARC) through

DP110103909 and Auto CRC 2020 are gratefully acknowledged. This research used a JSM-7500FA GENERAL field emission scanning electron microscope funded by Australian Research Council grant(s) and located at the University of Wollongong Electron Microscopy Centre. The synchrotron x-ray diffraction part of this work was conducted at powder diffraction beamline, Australian Synchrotron (Melbourne).The authors also want to thank Dr. Zhiping Lin, Dr. Jiazhao Wang, Mr. Fang Hong and Mr. Zengji Yue for their help and Dr. T. Silver for critical reading of the manuscript.

6. References

[1] J.B. Goodenough, Y. Kim, Challenges for rechargeable Li batteries, Chem. Mater. 22 (2010) 587-603.

[2] B.L. Ellis, W.R.M. Makahnouk, Y. Makimura, K. Toghill, L.F. Nazar, A multifunctional 3.5 V iron-based phosphate cathode for rechargeable batteries, Nat. Mater. 6 (2007) 749-753.

[3] L. Dimesso, C. Forster, W. Jaegermann, J.P. Khanderi, H. Tempel, A. Popp, J. Engstler, J.J. Schneider, A. Sarapulova, D. Mikhailova, L.A. Schmitt, S. Oswald, H. Ehrenberg, Developments in nanostructured $LiMPO_4$ (M = Fe, Co, Ni, Mn) composites based on three dimensional carbon architecture, Chem. Soc. Rev. 41 (2012) 5068-5080.

[4] J.T. Xu, S.X. Dou, H.K. Liu, L.M. Dai, Cathode materials for next generation lithium ion batteries, Nano Energy 2 (2013) 439-442.

[5] L. Adam, A. Guesdon, B. Raveau, A new lithium manganese phosphate with an original tunnel structure in the $A_2MP_2O_7$ family, J. Solid. State. Chem. 181 (2008) 3110-3115.

[6] S. Nishimura, M. Nakamura, R. Natsui, A. Yamada, New lithium iron pyrophosphate as 3.5 V class cathode material for lithium ion battery, J. Am. Chem. Soc. 132 (2010) 13596-13597.

[7] H. Zhou, S. Upreti, N.A. Chernova, G. Hautier, G. Ceder, M.S. Whittingham, Iron and manganese pyrophosphates as cathodes for lithium-ion batteries, Chem. Mater. 23 (2011)

293-300.

[8] P. Barpanda, S. Nishimura, A. Yamada, High-voltage pyrophosphate cathodes, Adv. Energy Mater. 2 (2012) 841-859.

[9] P. Barpanda, T. Ye, S.C. Chung, Y. Yamada, S. Nishimura, A. Yamada, Eco-efficient splash combustion synthesis of nanoscale pyrophosphate ($Li_2FeP_2O_7$) positive-electrode using Fe(III) precursors, J. Mater. Chem. 22 (2012) 13455-13459.

[10] J.M. Clark, S. Nishimura, A. Yamada, M.S. Islam, High-voltage pyrophosphate cathode: insights into local structure and lithium-diffusion pathways, Angew. Chem. Int. Ed. 51 (2012) 13149-13153.

[11] N. Furuta, S. Nishimura, P. Barpanda, A. Yamada, Fe^{3+}/Fe^{2+} redox couple approaching 4 V in $Li_{2-x}(Fe_{1-y}Mn_y)P_2O_7$ pyrophosphate cathodes, Chem. Mater. 24 (2012) 1055-1061.

[12] D. Shimizu, S. Nishimura, P. Barpanda, A. Yamada, Electrochemical redox mechanism in 3.5 V $Li_{2-x}FeP_2O_7$ ($0 \leq x \leq 1$) pyrophosphate cathode, Chem Mater. 24 (2012) 2598-2603.

[13] M. Tamaru, P. Barpanda, Y. Yamada, S. Nishimura, A. Yamada, Observation of the highest Mn^{3+}/Mn^{2+} redox potential of 4.45 V in a $Li_2MnP_2O_7$ pyrophosphate cathode, J. Mater. Chem. 22 (2012) 24526-24529.

[14] P. Barpanda, G. Rousse, T. Ye, C.D. Ling, Z. Mohamed, Y. Klein, A. Yamada, Neutron diffraction study of the Li-ion battery cathode $Li_2FeP_2O_7$, Inorg. Chem. 52 (2013) 3334-3341.

[15] J. Du, L.F. Jiao, Q. Wu, Y.C. Liu, Y.P. Zhao, L.J. Guo, Y.J. Wang, H.T. Yuan, Synthesis and characterization of $Li_2FeP_2O_7$/C nanocomposites as cathode materials for Li-ion batteries, Electrochim. Acta 103 (2013) 219-225.

[16] M. Tamaru, S.C. Chung, D. Shimizu, S. Nishimura, A. Yamada, Pyrophosphate chemistry toward safe rechargeable batteries, Chem. Mater. 25 (2013) 2538-2543.

[17] M. Saito, S. Yano, T. Maekawa, A. Tasaka, M. Inaba, Synthesis and electrochemical properties of carbon-coated $Li_2FeP_2O_7$ for Li-ion batteries, ECS Trans. 50 (2013) 251-259.

[18] S. Lee, S.S. Park, Structure, defect chemistry, and lithium transport pathway of lithium transition metal pyrophosphates ($Li_2MP_2O_7$, M: Mn, Fe, and Co): atomistic simulation study, Chem. Mater. 24 (2012) 3550-3557.

[19] S.-Y. Chung, J.T. Bloking, Y.-M. Chiang, electronically conductive phospho-olivines as lithium storage electrodes, Nat. Mater. 1 (2002) 123-128.

[20] N. Meethong, Y.H. Kao, S.A. Speakman, Y.M. Chiang, Aliovalent substitutions in olivine lithium iron phosphate and impact on structure and properties, Adv. Funct. Mater. 19 (2009) 1060-1070.

[21] Y.X. Wen, L.M. Zeng, Z.F. Tong, L.Q. Nong, W.X. Wei, Structure and properties of $LiFe_{0.9}V_{0.1}PO_4$, J. Alloy. Compd. 416 (2006) 206-208.

[22] X.J. Chen, G.S. Cao, X.B. Zhao, J.P. Tu, T.J. Zhu, Electrochemical performance of $LiFe_{1-x}VxPO_4$/carbon composites prepared by solid-state reaction, J. Alloy. Compd. 463 (2008) 385-389.

[23] T.S. Shi, H.M. Pei, Y.L. Shi, C.D. Xiao, Y.Y. Chun, Synthesis and electrochemical properties $Li_{1-x}V_xCr_yFe_{1-x}PO_4$/C as a cathode material, Chin. Chem. Lett. 19 (2008) 337-341.

[24] C.S. Sun, Z. Zhou, Z.G. Xu, D.G. Wang, J.P. Wei, X.K. Bian, J. Yan, Improved high-rate charge/discharge performances of $LiFePO_4$/C via V-doping, J. Power Sources 193 (2009) 841-845.

[25] N. Hua, C.Y. Wang, X.Y. Kang, T. Wumair, Y. Han, Studies of V doping for the $LiFePO_4$-based Li Ion batteries, J. Alloy. Compd. 503 (2010) 204-208.

[26] T. Zhao, W. Xu, Q. Ye, J. Cheng, H.F. Zhao, Z.Y. Wu, D.G. Xia, W.S. Chu, Local structure of vanadium in doped $LiFePO_4$, J. Synchrotron Radiat. 17 (2010) 584-589.

[27] Y. Jin, C.P. Yang, X.H. Rui, T. Cheng, C.H. Chen, V_2O_3 modified $LiFePO_4$/C composite with improved electrochemical performance, J. Power Sources 196 (2011) 5623-5630.

[28] J. Ma, B.H. Li, H.D. Du, C.J. Xu, F.Y. Kang, The effect of vanadium on

physicochemical and electrochemical performances of $LiFePO_4$ cathode for lithium battery, J. Electrochem. Soc. 158 (2011) A26-A32.

[29] F. Omenya, N.A. Chernova, S. Upreti, P.Y. Zavalij, K.W. Nam, X.Q. Yang, M.S. Whittingham, Can vanadium be substituted into $LiFePO_4$?, Chem. Mater. 23 (2011) 4733-4740.

[30] L.L. Zhang, G. Liang, A. Ignatov, M.C. Croft, X.Q. Xiong, I.M. Hung, Y.H. Huang, X.L. Hu, W.X. Zhang, Y.L. Peng, Effect of vanadium incorporation on electrochemical performance of $LiFePO_4$ for lithium-ion batteries, J. Phys. Chem. C, 115 (2011) 13520-13527.

[31] C.Y. Chiang, H.C. Su, P.J. Wu, H.J. Liu, C.W. Hu, N. Sharma, V.K. Peterson, H.W. Hsieh, Y.F. Lin, W.C. Chou, C.H. Lee, J.F. Lee, B.Y. Shew, Vanadium substitution of $LiFePO_4$ cathode materials to enhance the capacity of $LiFePO_4$-based lithium-ion batteries, J. Phys. Chem. C, 116 (2012) 24424-24429.

[32] V. Aravindan, W. Chuiling, S. Madhavi, Electrochemical performance of NASICON type carbon coated $LiTi_2(PO_4)_3$ with a spinel $LiMn_2O_4$ cathode, RSC Adv. 2 (2012) 7534-7539.

[33] G. Yang, C.Y. Jiang, X.M. He, J.R. Ying, F.P. Cai, Preparation of V-$LiFePO_4$ cathode material for Li-ion batteries, Ionics 18 (2012) 59-64.

[34] A. Moretti, G. Giuli, F. Nobili, A. Trapananti, G. Aquilanti, R. Tossici, R. Marassi, Structural and electrochemical characterization of vanadium-doped $LiFePO_4$ cathodes for lithium-ion batteries, J. Electrochem. Soc. 160 (2013) A940-A949.

[35] F. Omenya, N.A. Chernova, Q. Wang, R.B. Zhang, M.S. Whittingham, The structural and electrochemical impact of Li and Fe site substitution in $LiFePO_4$, Chem. Mater. 25 (2013) 2691-2699.

[36] F. Omenya, N.A. Chernova, R.B. Zhang, J. Fang, Y.Q. Huang, F. Cohen, N. Dobrzynski, S. Senanayake, W.Q. Xu, M.S. Whittingham, Why substitution enhances the reactivity of

$LiFePO_4$, Chem. Mater. 25 (2013) 85-89.

[37] T. Ohzuku, Y. Makimura, Layered lithium insertion material of $LiNi_{1/2}Mn_{1/2}O_2$: a possible alternative to $LiCoO_2$ for advanced lithium-ion batteries, Chem. Lett. 30 (2001) 744-745.

[38] J.K. Ngala, N.A. Chernova, M. Ma, M. Mamak, P.Y. Zavalij, M.S. Whittingham, The synthesis, characterization and electrochemical behavior of the layered $LiNi_{0.4}Mn_{0.4}Co_{0.2}O_2$ compound, J. Mater. Chem. 14 (2004) 214-220.

[39] K. Kang, Y.S. Meng, J. Breger, C.P. Grey, G. Ceder, Electrodes with high power and high capacity for rechargeable lithium batteries, Science 311 (2006) 977-980.

[40] J.T. Xu, S.L. Chou, Q.F. Gu, H.K. Liu, S.X. Dou, The effect of different binders on electrochemical properties of $LiNi_{1/3}Mn_{1/3}C_{1/3}O_2$ cathode material in lithium ion batteries, J. Power Sources 225 (2013) 172-178.

[41] D. Mohanty, A. Huq, E.A. Payzant, A.S. Sefat, J. Li, D.P. Abraham, D.L. Wood, C. Daniel, Neutron diffraction and magnetic susceptibility Studies on a high-voltage $Li_{1.2}Mn_{0.55}Ni_{0.15}Co_{0.10}O_2$ lithium ion battery cathode: insight into the crystal structure, Chem. Mater. 25 (2013) 4064-4070.

[42] Q. Kuang, Y.M. Zhao, X.N. An, J.M. Liu, Y.Z. Dong, L. Chen, Synthesis and electrochemical properties of Co-doped $Li_3V_2(PO_4)_3$ cathode materials for lithium-ion batteries, Electrochim. Acta 55 (2010) 1575-1581.

[43] C. Wurm, M. Morcrette, G. Rousse, L. Dupont, C. Masquelier, Lithium insertion/extraction into/from $LiMX_2O_7$ Compositions (M = Fe, V; X = P, As) prepared via a solution method, Chem. Mater, 14 (2002) 2701-2710.

[44] D. Aurbach, B. Markovsky, I. Weissman, E. Levi, Y. Ein-Eli, On the correlation between surface chemistry and performance of graphite negative electrodes for Li ion batteries, Electrochim. Acta 45 (1999) 67-86.

Table and Figures Captions

Table 1. Lattice parameters for $Li_2Fe_{1-3x/2}V_xP_2O_7$ (x = 0, 0.025, 0.05, 0.075, and 0.1) compounds.*

Table 2. Magnetic parameters of $Li_2Fe_{1-3x/2}V_xP_2O_7$ (x = 0, 0.025, and 0.05).*

Table 3. Kinetic parameters obtained from equivalent circuit fitting of experimental data from $Li_2Fe_{1-3x/2}V_xP_2O_7$ (x = 0, 0.025, 0.05, 0.075, and 0.1).

Figure 1. Synchrotron X-ray diffraction (SXRD) patterns for $Li_2Fe_{1-3x/2}V_xP_2O_7$ (a) x = 0, (b) x = 0.025, (c) x = 0.05, (d) x = 0.075 and (e) x = 0.1.

Figure 2. Lattice parameters (a) and unit cell volume (b) of $Li_2Fe_{1-3x/2}V_xP_2O_7$ (x = 0, 0.025, 0.05, 0.075, and 0.1).

Figure 3. Crystal structure of $Li_2Fe_{1-3x/2}V_xP_2O_7$.

Figure 4. (a) Magnetic susceptibility of $Li_2Fe_{1-3x/2}V_xP_2O_7$ (x = 0, 0.025, and 0.05) from 2 to 300 K; inset shows inverse susceptibilities corrected for temperature-independent contribution and their fit to the Curie Weiss law, and (b) low temperature magnetic susceptibility of $Li_2Fe_{1-3x/2}V_xP_2O_7$ (x = 0, 0.025, and 0.05); inset shows their dM/dT.

Figure 5. SEM images at low (a) and high magnification (b), TEM images at low (c) and high magnification (d) of $Li_2Fe_{1-3x/2}V_xP_2O_7$ (x = 0.025). Inset of Figure (d): Fourier transform image of (d).

Figure 6. (a) Thermogravimetric analysis (TGA) and (b) differential scanning calorimetry (DSC) plots of $Li_2Fe_{1-3x/2}V_xP_2O_7$ (x = 0, 0.025, 0.05, 0.075, and 0.1).

Figure 7. (a) Initial charge-discharge curves of $Li_2Fe_{1-3x/2}V_xP_2O_7$ (x = 0, 0.025, 0.05, 0.075, and 0.1) at 0.1 C in the voltage range of 2.0 - 4.5 V; and (b) rate capability vs. cycle number of $Li_2Fe_{1-3x/2}V_xP_2O_7$ (x = 0, 0.025, 0.05, 0.075, and 0.1) at different current densities in the voltage range of 2.0 - 4.5 V.

Figure 8. Cycling performance of $Li_2Fe_{1-3x/2}V_xP_2O_7$ (x = 0, 0.025, 0.05, 0.075, and 0.1) at 1 C in the voltage range of 2.0 - 4.5 V.

Figure 9. (a) Impedance plots for $Li_2Fe_{1-3x/2}V_xP_2O_7$ (x = 0, 0.025, 0.05, 0.075, and 0.1) electrodes measured after 25 cycles from 1 MHz to1 mHz; inset: equivalent circuit used for the EIS analysis; (b) magnification of (a).

Figure 1.

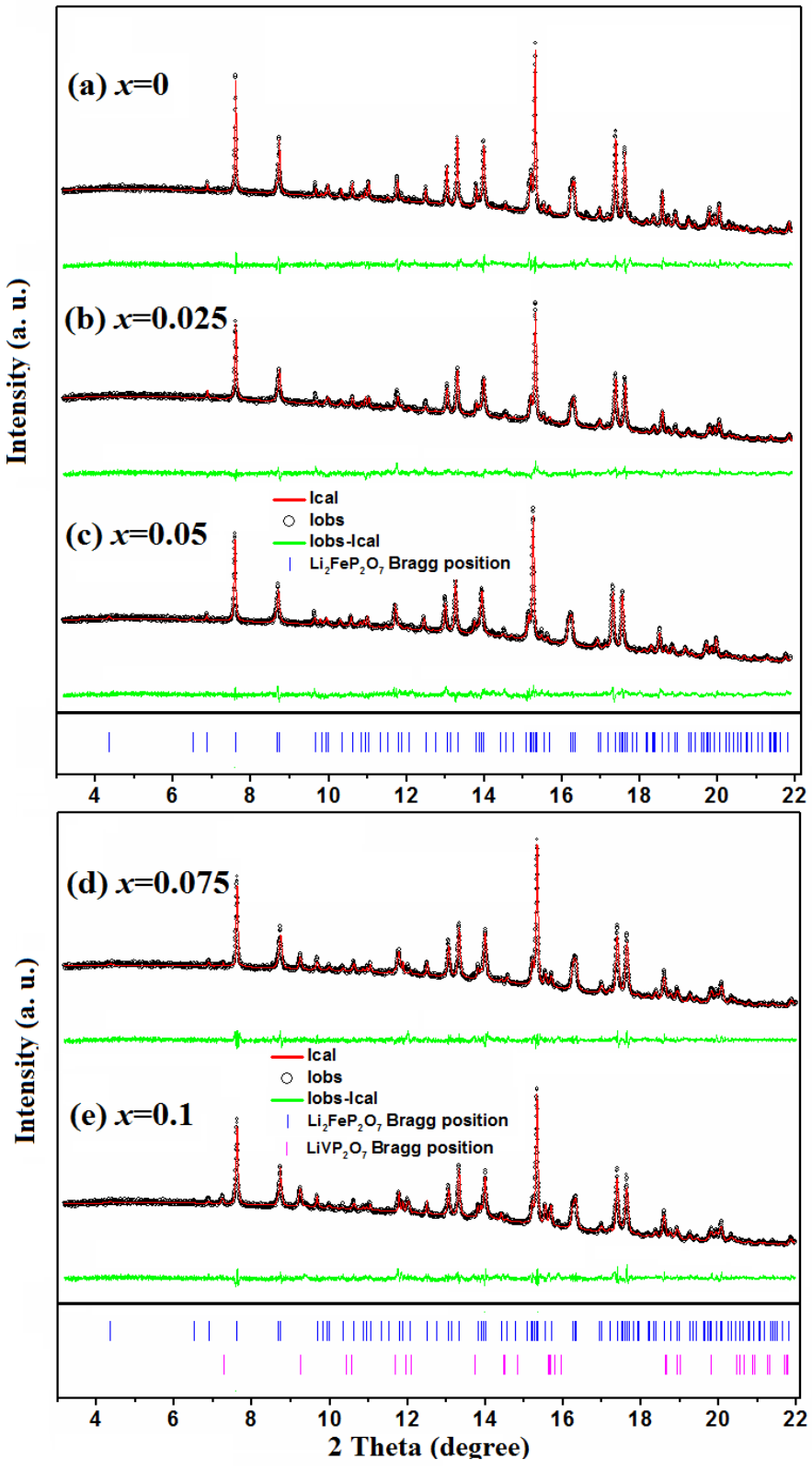
(a) x=0
(b) x=0.025
(c) x=0.05
(d) x=0.075
(e) x=0.1
Intensity (a. u.)
Intensity (a. u.)
Ical
Iobs
Iobs-Ical
Li2FeP2O7 Bragg position
LiVP2O7 Bragg position
4
6
8
10
12
14
16
18
20
22
2 Theta (degree)

Figure 2.

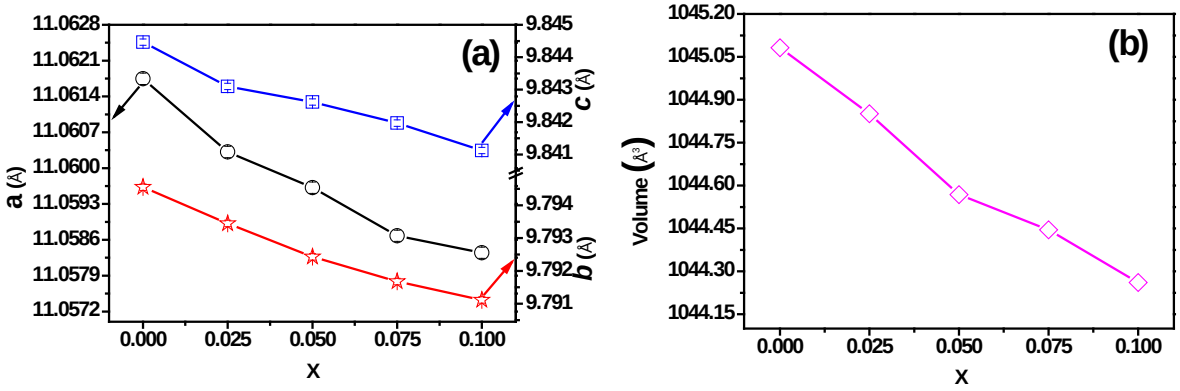
(a)
11.0628
11.0621
11.0614
11.0607
11.0600
11.0593
11.0586
11.0579
11.0572
a (Å)
9.845
9.844
9.843
9.842
9.841
9.794
9.793
9.792
9.791
c (Å)
b (Å)
0.000
0.025
0.050
0.075
0.100
x
(b)
1045.20
1045.05
1044.90
1044.75
1044.60
1044.45
1044.30
1044.15
Volume (Å³)
0.000
0.025
0.050
0.075
0.100
x

Figure 3.

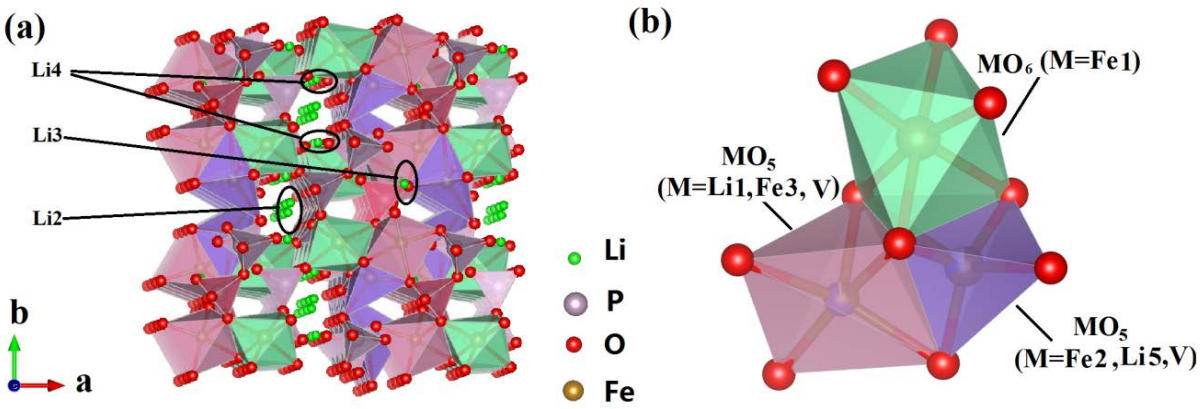

Figure 4.

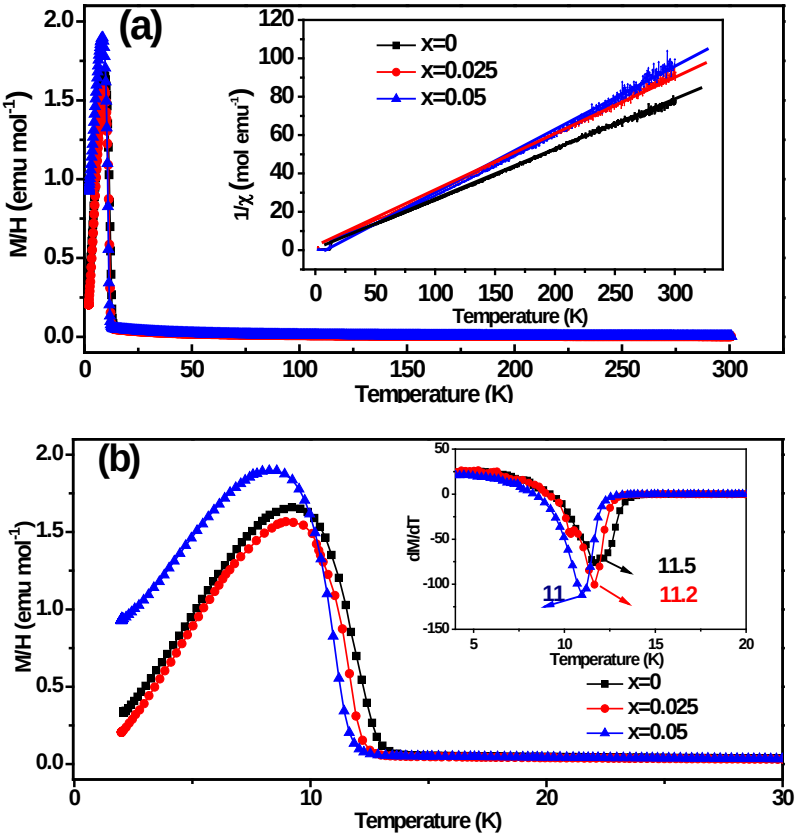
(a)
M/H (emu mol-1)
Temperature (K)
1/χ (mol emu-1)
x=0
x=0.025
x=0.05
(b)
M/H (emu mol-1)
Temperature (K)
dM/dT
11
11.5
11.2
x=0
x=0.025
x=0.05

Figure 5.

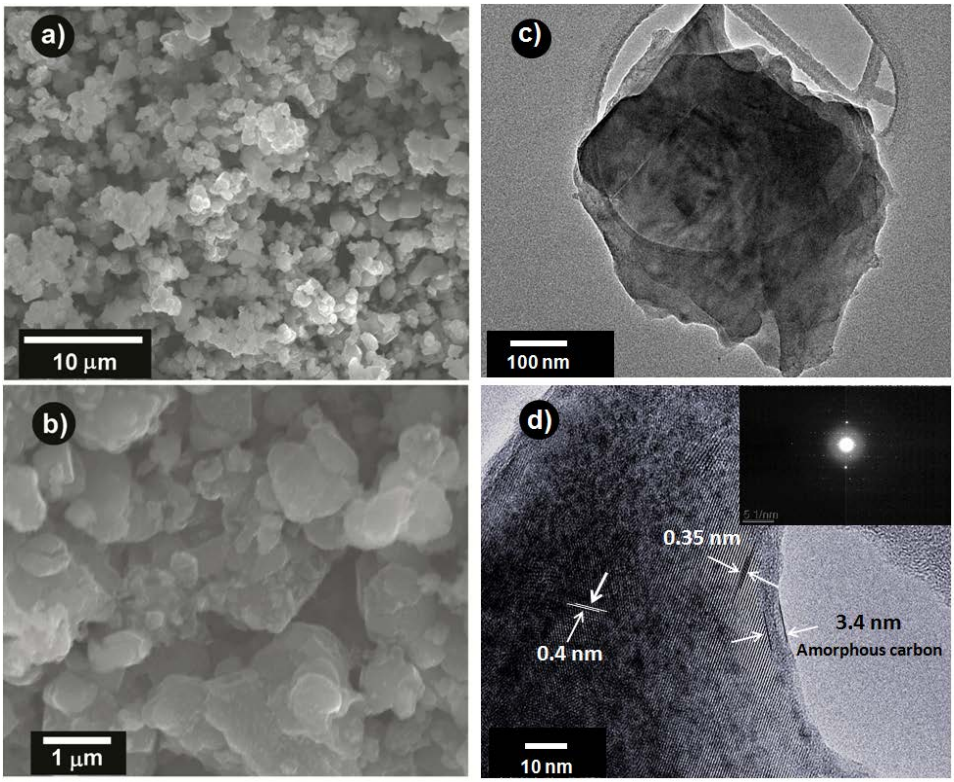

Figure 6.

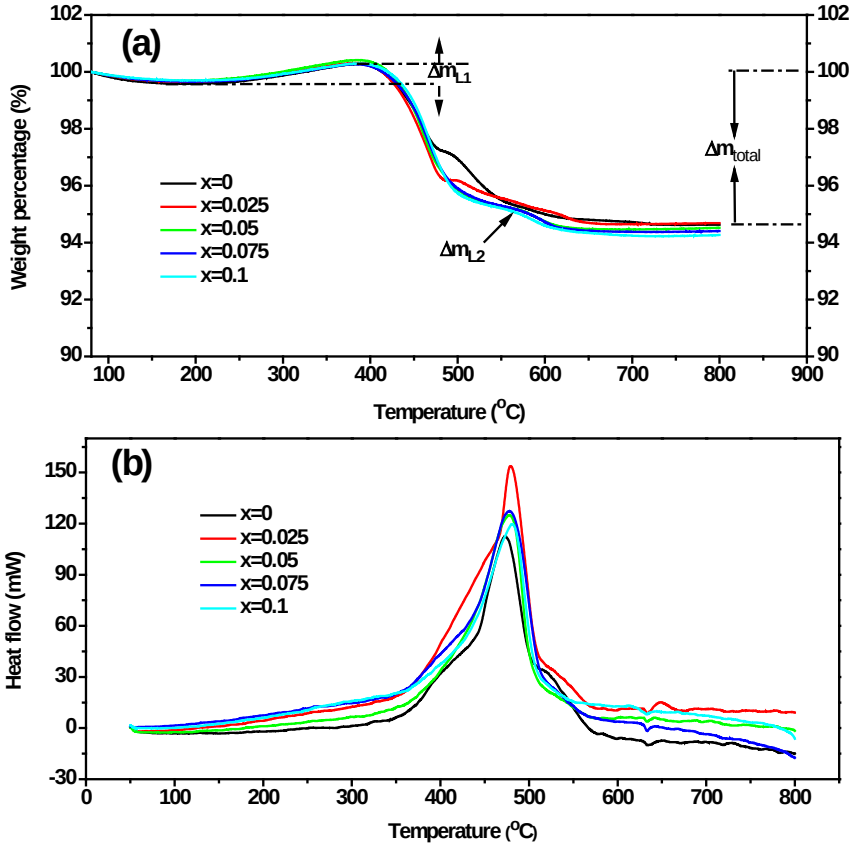
(a)
Weight percentage (%)
Temperature (°C)
x=0
x=0.025
x=0.05
x=0.075
x=0.1
Δm_L1
Δm_L2
Δm_total
(b)
Heat flow (mW)
Temperature (°C)
x=0
x=0.025
x=0.05
x=0.075
x=0.1

Figure 7.

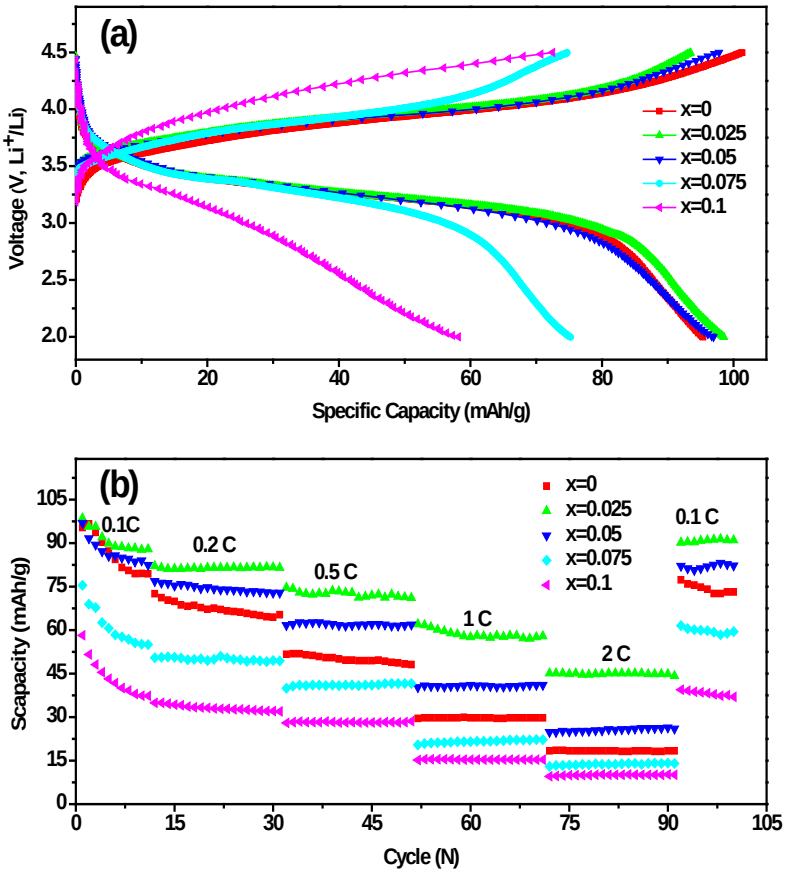
(a)
Voltage (V, Li+/Li)
Specific Capacity (mAh/g)
x=0
x=0.025
x=0.05
x=0.075
x=0.1
(b)
Scapacity (mAh/g)
Cycle (N)
0.1C
0.2 C
0.5 C
1 C
2 C
0.1 C

Figure 8.

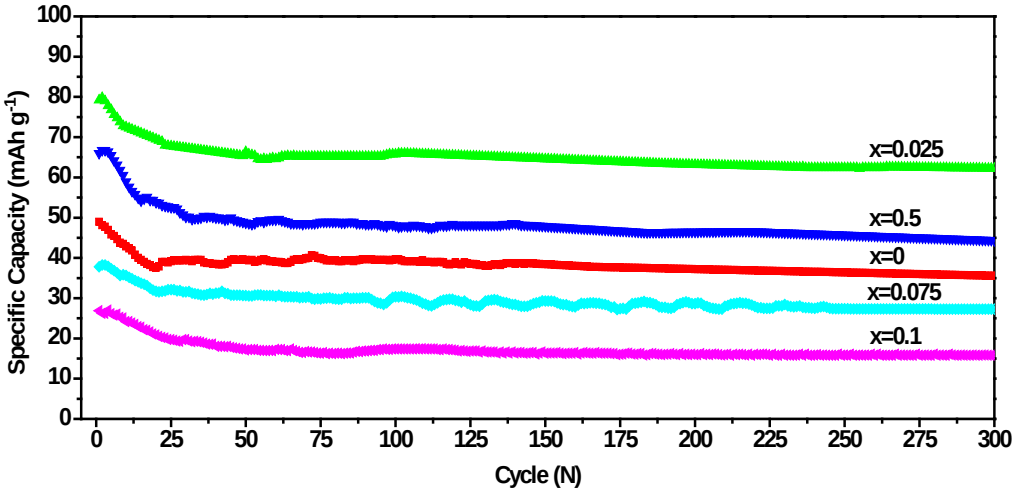
Specific Capacity (mAh g-1)
Cycle (N)
x=0.025
x=0.5
x=0
x=0.075
x=0.1
0
10
20
30
40
50
60
70
80
90
100
0
25
50
75
100
125
150
175
200
225
250
275
300

Figure 9.

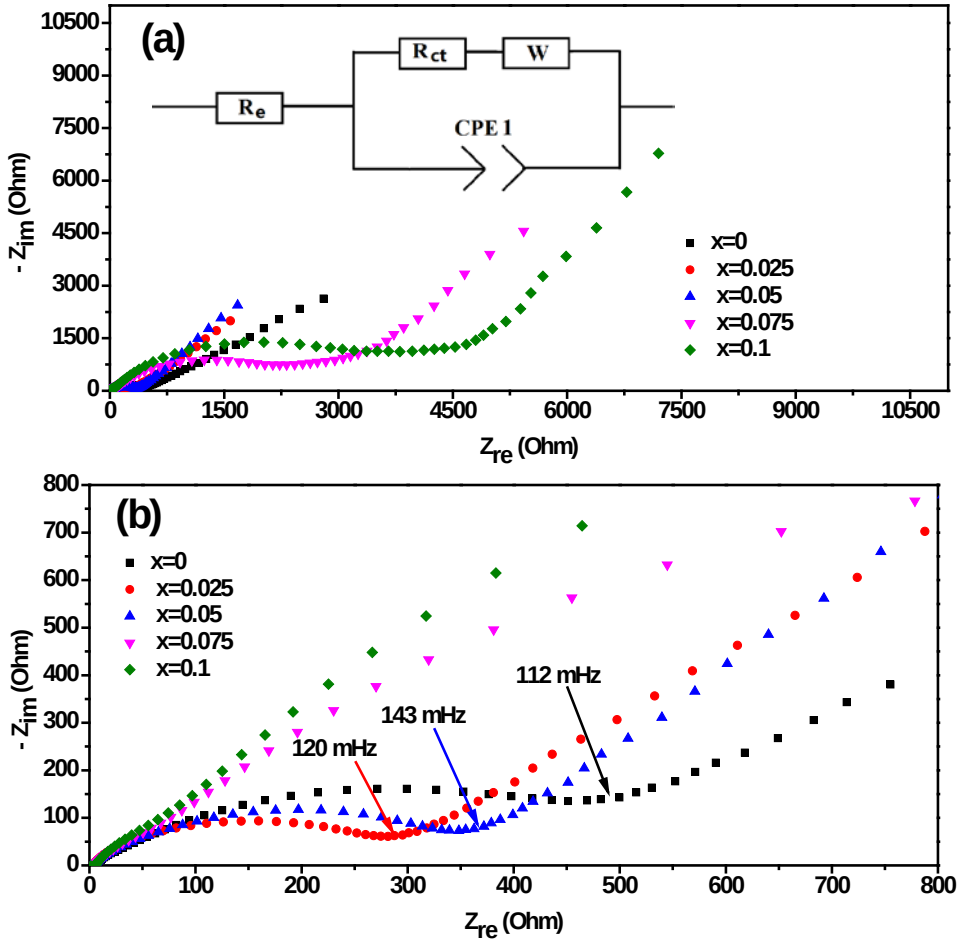
(a)
R_ct
W
R_e
CPE 1
x=0
x=0.025
x=0.05
x=0.075
x=0.1
- Z_im (Ohm)
Z_re (Ohm)
(b)
112 mHz
143 mHz
120 mHz

Table 1.

Samples	*a* (Å)	*b* (Å)	*c* (Å)	*β* (°)	Volume (Å^3)	R_p (%)	R_{wp} (%)	x^2
$x = 0$	11.0617(1)	9.7945(2)	9.8446(1)	101.52(1)	1045.082(1)	1.98	2.64	3.12
$x = 0.025$	11.0603(1)	9.7934(2)	9.8430(1)	101.48(0)	1044.851(2)	2.08	2.76	3.39
$x = 0.05$	11.0596 (1)	9.7924(0)	9.8426(2)	101.47(0)	1044.674(1)	2.43	3.35	5.04
$x = 0.075$	11.0586 (2)	9.7916(2)	9.8419(1)	101.46(1)	1044.445(3)	2.63	3.42	5.20
$x = 0.1$	11.0583(1)	9.7911(3)	9.8413(2)	101.46(1)	1044.261(2)	3.11	4.44	6.09

* The profile, R_p, and weighted profile, R_{wp}, R-factors and the goodness of fit, χ^2, are the agreement factors for the SXRD refinements of $Li_2Fe_{1-3x/2}V_xP_2O_7$ (x = 0, 0.025, 0.05, 0.075, and 0.1).

Table 2.

x	T_N (K)	C_M (emu K mol^{-1})	$\mu_{experiment}$ (μB)	μ_{theory} (μB)
0	11.5	2.98	4.88	4.90
0.025	11.2	2.84	4.77	4.79
0.05	11	2.71	4.66	4.67

* T_N is determined as an inflection point of the $M(T)$ dependence; experimental $\mu_{experiment}$ is determined using $\mu_{experiment} = [8C_M]^{1/2}$; in calculations of μ_{theory}, the magnetic moment of Fe^{2+} is calculated using $\mu_{theory} = 2[(S(S + 1))]^{1/2}$ ($S = 2$) = 4.9 μ_B, where S is the spin angular momentum. The effective magnetic moments for the intermediate compositions can be calculated as $\mu_{theory} = (1 - 3x/2)\mu_{theory}$ (Fe^{2+}) + $x\mu_{theory}$ (V^{3+}). The average effective magnetic moment per transition metal ion is calculated assuming that iron has the same magnetic moment as in $Li_2FeP_2O_7$ and that vanadium is in the 3^+ oxidation state ($S = 1$, $\mu_{theory} = 2.82$ μ_B), as suggested.

Table 3.

x	R_s/ Ω	R_{ct}/ Ω
0	4.2	480.8
0.025	3.8	262.9
0.05	3.6	356.8
0.075	4.6	2833
0.1	4.7	4392